VI$_3$: A two-dimensional Ising ferromagnet

Ke Yang,[1] Fengren Fan,[1] Hongbo Wang [ORCID],[2] D. I. Khomskii,[3] and Hua Wu [ORCID][1,4,*]

[1]*Laboratory for Computational Physical Sciences (MOE), State Key Laboratory of Surface Physics,
and Department of Physics, Fudan University, Shanghai 200433, China*
[2]*Laboratory of Advanced Materials Physics and Nanodevices, School of Physics and Technology, University of Jinan, Jinan 250022, China*
[3]*Institute of Physics II, University of Cologne, 50937 Cologne, Germany*
[4]*Collaborative Innovation Center of Advanced Microstructures, Nanjing 210093, China*

Two-dimensional (2D) magnetic materials are of great current interest for their promising applications in spintronics. Here we propose the van der Waals (vdW) material VI$_3$ to be a 2D Ising ferromagnet (FM), using density functional calculations, crystal field level diagrams, superexchange model analyses, and Monte Carlo simulations. The $a_{1g}\,^1 e'^1_-$ ground state in the trigonal crystal field gives rise to the 2D Ising FM due to a significant single ion anisotropy (SIA) and enhanced FM superexchange both associated with the $S_z = 1$ and $L_z = -1$ states of V^{3+} ions. We find that a tensile strain on the VI$_3$ monolayer further stabilizes the $a_{1g}\,^1 e'^1_-$ ground state, and its Curie temperature (T_C) would increase from 70 to 90–110 K under a 2.5%–5% tensile strain. Moreover, we suggest a group of spin-orbit states with a strong SIA which may help to search more 2D Ising magnets.

Two-dimensional (2D) crystals with intrinsic magnetism have been of great interest since the experimental achievements of the atomically thin CrI$_3$ [1] and Cr$_2$Ge$_2$Te$_6$ [2] flakes by exfoliation of bulk crystals. Through magneto-optical Kerr effects, the CrI$_3$ monolayer and Cr$_2$Ge$_2$Te$_6$ atomic layers have been demonstrated to be a ferromagnet (FM) with out-of-plane spin orientation. More recently, exfoliated Fe$_3$GeTe$_2$ monolayers have T_C above room temperature via ionic gating [3]. Those 2D FMs provide unique opportunities for understanding, exploring, and utilizing novel low-dimensional magnetism. Due to the thickness of one or few monolayers, one may be able to control the 2D magnetic properties by applying weak magnetic field [4–6], electric field [4,5], doping [3,7], or heterostructure [8,9]. This flexibility causes enormous excitement about their promising applications in spintronics.

Very recently, VI$_3$ emerges as a new 2D material with a similar van der Waals (vdW) layered structure as CrI$_3$ which is currently under extensive study [1,4–13]. The bulk material of VI$_3$ has been studied by several groups [14–20], and it is found to be an interesting FM insulator with $T_C \approx 50$ K and the easy magnetization c axis [14,15]. Note that CrI$_3$ has a closed t^3_{2g} shell for the octahedral Cr^{3+} $S = 3/2$ ion. Therefore, its orbital singlet produces no single ion anisotropy (SIA), and its finite perpendicular magnetic anisotropy comes from the exchange anisotropy caused by the spin-orbit coupling (SOC) of the heavy I $5p$ orbitals and their hybridization with the Cr $3d$ [12,13]. In contrast, VI$_3$ has an open t^2_{2g} shell for the $S = 1$ V^{3+}, and therefore it has room to achieve an orbital moment and a consequent strong SIA due to SOC. Then, VI$_3$ may be an Ising-type 2D FM.

In this Rapid Communication, we indeed find that the insulating VI$_3$ vdW monolayer has the $a_{1g}\,^1 e'^1_-$ ground state with $S_z = 1$ and $L_z = -1$ in the trigonal crystal field. The FM superexchange and the strong perpendicular SIA produce the 2D Ising FM. The $a_{1g}\,^1 e'^1_-$ ground state can further be stabilized by a tensile strain, which would enhance T_C of the VI$_3$ monolayer from 70 to 90–110 K under 2.5%–5% strain. Therefore, the VI$_3$ monolayer could be the first real 2D Ising FM insulator, which calls for a prompt experimental verification.

We have carried out density functional theory (DFT) calculations for both bulk and monolayer VI$_3$, using the experimental lattice parameters [14] and the full-potential augmented plane wave plus local orbital code (WIEN2K) [21] (see more computational details in the Supplemental Material [22]). To account for the electron correlation of the narrow V $3d$ bands, the local-spin-density approximation plus Hubbard U (LSDA+U) calculations were performed using Hubbard $U = 4.0$ eV and Hund exchange $J_H = 0.9$ eV [23]. The SOC is included for both V $3d$ and I $5p$ orbitals by the second-variational method. As seen below, the SOC is crucial and any reasonable U (e.g., 2–5 eV) is big enough to open an insulating gap between the SOC split $e'_\pm$ states and hence reach the same ground state solution for VI$_3$. Moreover, we have used the crystal field and superexchange pictures to understand the 2D Ising FM in VI$_3$ as detailed below. Furthermore, we have estimated the T_C of the VI$_3$ monolayer using Monte Carlo (MC) simulations on a $6 \times 6 \times 1$ spin matrix. At each temperature, 2.4×10^7 MC steps/site were performed to reach an equilibrium using the Metropolis method [24], and then the specific heat is calculated.

We first consider the situation in the bulk VI$_3$ where some recent experimental results [14,15] are available for comparison. According to the crystal structure of the bulk VI$_3$ in the $R\bar{3}$ space group [14], the V ions have a local
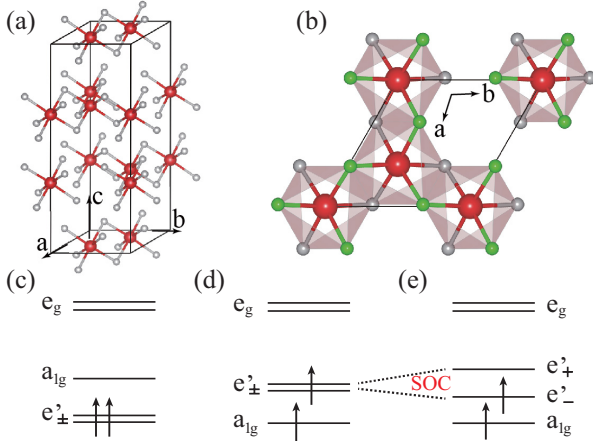
---

*Corresponding author: wuh@fudan.edu.cn

100402-1

FIG. 1. (a) The bulk crystal structure of VI_3, with V (I) atoms represented by red (gray) balls. (b) The honeycomb V lattice of the VI_3 monolayer, and the green (gray) balls standing for the I atoms above (below) the V layer, forming the edge-sharing VI_6 octahedra. (c) The $e'^2_\pm$ or (d) a_{1g} $^1e'^1_\pm$ configuration for the V^{3+} $S = 1$ ion in the trigonal crystal field level diagrams, with the active SOC effect in (e).

TABLE I. Relative total energies ΔE (meV/f.u.) by LSDA+SOC+U, local spin, and orbital moments (μ_B) for the V^{3+} ion. The perpendicular magnetization is assumed in most cases, and the in-plane magnetization is also set for a_{1g} $^1e'^1_-$. The corresponding data for the fully relaxed structures are listed in the round brackets.

VI_3 bulk		ΔE	M_{spin}	M_{orb}
a_{1g} $^1e'^1_-$	FM	0.0 (0.0)	1.89 (1.86)	−1.05 (−1.00)
	AF	21.3	1.85	−1.07
a_{1g} $^1e'^1_+$	FM	38.7	1.89	1.03
$e'^2_\pm$	FM	9.3 (11.8)	1.83 (1.80)	0.05 (0.05)
	AF	15.8	1.81	0.07
VI_3 monolayer		ΔE	M_{spin}	M_{orb}
a_{1g} $^1e'^1_-$	FM	0.0 (0.0)	1.88 (1.84)	−1.08 (−1.04)
	AF	20.2 (20.0)	1.84 (1.80)	−1.09 (−1.05)
a_{1g} $^1e'^1_-$	FM	17.0 (17.6)	1.88 (1.84)	−0.15 (−0.15)
(in-plane M)	AF	35.2 (33.9)	1.84 (1.80)	−0.14 (−0.17)
$e'^2_\pm$	FM	20.1 (45.5)	1.82 (1.78)	0.05 (0.05)
	AF	27.1 (52.5)	1.80 (1.76)	0.07 (0.07)

octahedral coordination but a trigonal crystal field in the global coordinate system, which splits the otherwise degenerate t_{2g} triplet into the a_{1g} singlet and $e'_\pm$ doublet (see Fig. 1). Several very recent DFT studies gave conflicting results for the bulk VI_3 (either metallic [14,25] or insulating [15,16]), but so far no understanding of the perpendicular FM has been available. In the DFT+U framework one may readily get the insulating solution with the $e'^2_\pm$ double occupation, in contrast to the metallic state a_{1g} $^1e'^1_\pm$ with the half-filled $e'_\pm$ doublet. However, it is the half-filled $e'_\pm$ doublet [Figs. 1(d) and 1(e)] which makes the SOC active and may eventually determine the perpendicular FM. For this purpose, we have carried out LSDA+SOC+U calculations for the bulk VI_3 to make a direct comparison between two configurations, $e'^2_\pm$ and a_{1g} $^1e'^1_\pm$. These two configurations are initialized via the occupation density matrix over the eigenorbitals [26,27], rather than a common representation by the two doublets (xy, x^2-y^2) and (xz, yz) in the trigonal crystal field, which may not find the correct a_{1g} $^1e'^1_-$ ground state in the calculations.

Our LSDA+SOC+U calculations show that both insulating solutions can be stabilized, and that the a_{1g} $^1e'^1_-$ state, now with $l_z = -1$, is more stable than the $e'^2_\pm$ state, by 9.3 meV/f.u., as seen in Table I. Both the solutions have the local V^{3+} spin moment more than $1.8\mu_B$ and the total spin moment of $2\mu_B$/f.u., showing exactly the formal V^{3+} $S = 1$ state. Note that the former solution has now a large orbital moment of $-1.05\mu_B$ along the z axis due to filling of the lower e'_- ($l_z = -1$) level after the SOC splitting of the $e'_\pm$ doublet [Fig. 1(e)]. In contrast, the fully occupied $e'^2_\pm$ doublet has no orbital degree of freedom and thus only a very small orbital moment of $0.05\mu_B$ is induced by the SOC. To prove the essential role of the SOC, we have also calculated the a_{1g} $^1e'^1_+$ state with filling of the SOC-split upper e'_+ ($l_z = 1$) level. The resulting total energy rises by 38.7 meV/f.u., compared with the a_{1g} $^1e'^1_-$ ground state. Then the SOC parameter of the V^{3+} ion $\xi = 38.7$ meV is derived, and it is (largely) responsible for

the energy lowering of the a_{1g} $^1e'^1_-$ ground state, relative to the $e'^2_\pm$ state where the SOC is almost absent. Note that the SOC parameter ξ is partially enhanced [28,29] here by the strong SOC of the heavy I atom via the I $5p$–V $3d$ hybridization.

Moreover, for both insulating solutions, a_{1g} $^1e'^1_-$ and $e'^2_\pm$, the FM state is more stable than the antiferromagnetic (AF) state (see Table I). While the FM stability against AF is 6.5 meV/f.u. for the $e'^2_\pm$ state, it increases a lot to 21.3 meV/f.u. for the a_{1g} $^1e'^1_-$ ground state. This enhanced FM superexchange in the a_{1g} $^1e'^1_-$ ground state appears also in the VI_3 monolayer and will be explained below. The FM order can further be stabilized by its Ising-type magnetism due to the SOC between the $S_z = 1$ and $L_z = -1$. The total magnetic moment of about $1\mu_B$/f.u. is strongly reduced from the V^{3+} $S = 1$ state, and it well accounts for the experimental easy z-axis magnetization of $1–1.3\mu_B$ in the FM insulating VI_3 [14,15].

As VI_3 bulk has already the potential to be an Ising FM, its vdW monolayers could well be a 2D Ising FM, with a better tunability. The cleavage energy is calculated to be 0.27 J/m^2 (see Supplemental Material [22]), using DFT+vdW corrections within the Grimme's approach [30], and it is well comparable to those for other 2D materials such as CrI_3 (0.30 J/m^2) [10], $Cr_2Si_2Te_6$ (0.35 J/m^2), and $Cr_2Ge_2Te_6$ (0.38 J/m^2) [31]. Therefore, an exfoliation of the VI_3 monolayer is likely, and we now switch to the treatment of the VI_3 monolayer.

Our local density approximation (LDA) and local spin density approximation (LSDA) calculations find a FM metallic solution, and LSDA+U calculations give a FM insulating solution with $e'^2_\pm$ (see Supplemental Material [22]). One may assume that the experimental FM insulating behavior is reproduced by the $e'^2_\pm$ state. However, a key point is the following: the V^{3+} $e'^2_\pm$ state has only the pure $S = 1$ and a quenched orbital moment, i.e., no SIA which would be very beneficial for the 2D FM. Apparently, such a solution would hardly explain the strong perpendicular FM observed in bulk VI_3
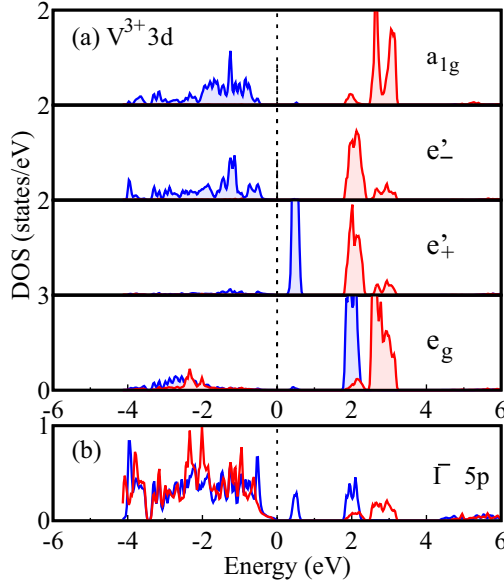
FIG. 2. The a_{1g} $^1e'^1_-$ ground state with a strong V $3d$–I $5p$ hybridization by LSDA+SOC+U. The blue (red) curves stand for the up (down) spin. Fermi level is set at zero energy.

[14,15]. Then, one may have to resort, as in the extensively studied CrI$_3$ [12,13], to the weak exchange anisotropy due to the SOC of the I $5p$ orbital and its hybridization with V $3d$. But actually, VI$_3$ has a more than one order of magnitude stronger SIA, which determines its 2D Ising FM as demonstrated below.

Our LSDA+SOC+U calculations give the insulating a_{1g} $^1e'^1_-$ ground state (Fig. 2), with the gap opening due to the electron correlation within the SOC-split $l_z = \pm 1$ states, and it is more stable than the $e'^2_\pm$ solution by 20.1 meV/f.u. (see Table I). Note that for the partially filled t_{2g} systems, there is an old and well-known dichotomy (see., e.g., Ref. [32]): such ions, on one hand, are Jahn-Teller (JT) active and may distort and fill orbitals according to the JT scenario; here for V^{3+} $3d^2$ occupation, giving the $e'^2_\pm$ state. But they can also form the
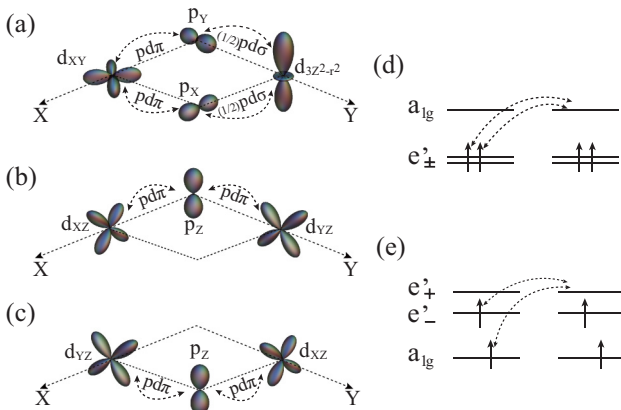

FIG. 3. Schematic plot of the hopping channels involved in the (near-) 90° FM superexchange: (a) d_{XY}-(p_X, p_Y)-$d_{3Z^2-r^2}$, (b) d_{XZ}-p_Z-d_{YZ}, and (c) d_{YZ}-p_Z-d_{XZ}. Virtual hoppings between the V^{3+} ions with (d) $e'^2_\pm$ and (e) a_{1g} $^1e'^1_-$ 1.

state with unquenched orbital moment and gain extra SOC energy. The above results imply that the SOC effects, from V $3d$ itself and I $5p$ via the p-d hybridization (see Fig. 2), indeed favor the a_{1g} $^1e'^1_-$ ground state solution.

Moreover, for the a_{1g} $^1e'^1_-$ ground state, the FM state is more stable than the AF state by 20.2 meV/f.u., which is very similar to the bulk case (see Table I). In contrast, for the $e'^2_\pm$ state, the FM state is more stable than the AF state only by 7.0 meV/f.u. Here we provide a picture to understand the enhanced FM superexchange in the a_{1g} $^1e'^1_-$ ground state. Considering the honeycomb lattice of the V^{3+} magnetic ions and the edge-sharing VI$_6$ octahedral network (see Fig. 1), we discuss the near-90° FM superexchange interactions (see Fig. 3). Here we choose a local octahedral XYZ coordinate system, with the XYZ axes directed from V to neighboring I ions. Then the local octahedral t_{2g} triplet under a trigonal crystal field can be expressed as

$$a_{1g} = \frac{1}{\sqrt{3}}(XY + XZ + YZ),$$

$$e'_+ = \frac{1}{\sqrt{3}}(XY + e^{i2\pi/3}XZ + e^{i4\pi/3}YZ), \quad (1)$$

$$e'_- = \frac{1}{\sqrt{3}}(XY + e^{i4\pi/3}XZ + e^{i2\pi/3}YZ).$$

The V-V superexchange contains several contributions. In analogy with the well-studied CrI$_3$, the main FM contribution comes from the occupied t_{2g}-empty e_g virtual hoppings [11]. There are also AF processes, due to hoppings between the occupied t_{2g} orbitals. Importantly, in VI$_3$, and in contrast to CrI$_3$, there appear the FM contributions due to hoppings from occupied to empty t_{2g} orbitals; these will turn out to be crucial in enhancing FM contributions for the a_{1g} $^1e'^1_-$ ground state.

We schematically illustrate these contributions treating VI$_3$ as a Mott-Hubbard (MH) insulator. Actually for such ligand as I the system may be close to a charge-transfer (CT) regime (see, e.g., Ref. [32]); this would add extra terms in the superexchange, but this would not change the main conclusions here. In the MH regime the main superexchange occurs due to the effective d-d hoppings through the same $5p$ orbital of I ions (in the CT case also the hoppings via different orthogonal $5p$ orbitals could enter). The main FM contribution comes from the effective V-V hopping from each of the above three orbitals to the neighboring empty (real) e_g orbital $3Z^2$-r^2 via the mechanism shown in Fig. 3(a) (the hoppings to the X^2-Y^2 orbital via two iodine ions cancel due to the signs of the d- and p-wave functions). According to Fig. 3(a), only the XY component of each of the states in Eq. (1) is active here, and the hoppings from each of them to the $3Z^2$-r^2 orbital of a neighboring V are equal, and we see that this FM contribution is the same for both the a_{1g} $^1e'^1_-$ and $e'^2_\pm$ configurations.

As mentioned above, also for t_{2g}-t_{2g} contributions, the V-V hopping and superexchange via the common single $5p_z$ orbital of two I$^-$ ligands, as sketched in Figs. 3(b) and 3(c), are also effective. Then we have the effective hoppings as follows:

$$\langle a_{1g}|\hat{t}|a_{1g}\rangle = -2t_0, \quad \langle e'_+|\hat{t}|e'_+\rangle = \langle e'_-|\hat{t}|e'_-\rangle = -t_0,$$
$$\langle e'_+|\hat{t}|e'_-\rangle = -2t_0, \quad \langle a_{1g}|\hat{t}|e'_+\rangle = \langle a_{1g}|\hat{t}|e'_-\rangle = -t_0, \quad (2)$$

where $t_0 = t_{pd\pi}^2/(3\Delta)$ and Δ is the charge-transfer energy. Using these hoppings, one can show that the AF contribution due to hopping between occupied t_{2g} orbitals is again the same for both $a_{1g}\,{}^1e'_-^1$ and $e'^2_\pm$. This is, however, not the case for the FM t_{2g}-t_{2g} contribution. Then, for the $e'^2_\pm$ state [Fig. 3(d)], the FM superexchange due to the above hoppings gains the energy against the AF by $(4t_0^2/U)(2J_H/U)$. But for the $a_{1g}\,{}^1e'_-^1$ ground state [Fig. 3(e)], the corresponding energy gain is more than doubled, $(10t_0^2/U)(2J_H/U)$. This could be a major reason why the $a_{1g}\,{}^1e'_-^1$ ground state has a much enhanced FM superexchange as compared to $e'^2_\pm$, as shown in the above LSDA+SOC+U calculations.

Note that the $a_{1g}\,{}^1e'_-^1$ ground state has a local V^{3+} spin moment of $1.88\mu_B$ and an antiparallel orbital moment of $-1.08\mu_B$ along the z axis, i.e., the SOC aligns the magnetic moment along the z axis via the strong SIA, thus producing the perpendicular magnetic anisotropy and the resulting Ising magnetism. Here we assume the spin Hamiltonian

$$H = -\frac{J}{2}\sum_{i,j}\vec{S}_i \cdot \vec{S}_j - D\sum_i \left(S_i^z\right)^2 - \frac{J'}{2}\sum_{i,j}S_i^z \cdot S_j^z, \quad (3)$$

where the first term describes the Heisenberg isotropic exchange (FM when $J > 0$), the second term is the SIA with the easy magnetization z axis (when $D > 0$), and the last term refers to the anisotropic exchange (the easy z axis when $J' > 0$). For the VI$_3$ monolayer, the sum over i runs over all V^{3+} atoms with $S = 1$ in the honeycomb lattice, and j over the three first nearest V^{3+} neighbors of each i. We have estimated the three magnetic parameters J, D, and J', by calculating four different magnetic states, FM and AF with the perpendicular or in-plane magnetization (see Table I). The total energy results allow us to estimate $J = 6.07$ meV, $D = 15.9$ meV, and $J' = 0.67$ meV. We see that the perpendicular magnetic anisotropy of the VI$_3$ monolayer arises predominantly from the D term, i.e., from the strong Ising-type SIA. This is one of the main results of this Rapid Communication. With these three parameters, our Monte Carlo simulations find that T_C of the VI$_3$ monolayer would be 40 K with the J-J' contributions, 68 K with the J-D contributions, and 74 K with the J-D-J' contributions. Therefore, the D contribution is about five times stronger than J' in stabilizing the 2D FM order.

The above results remain largely unchanged when we carry out a structural optimization for the VI$_3$ monolayer (see Table I). The only significant change is that the insulating $a_{1g}\,{}^1e'_-^1$ ground state, at the theoretical equilibrium lattice constant $a = b = 6.70$ Å (as compared with the experimental bulk value $a = b = 6.88$ Å [14]), becomes even more stable than the $e'^2_\pm$ state, by 45.5 meV/f.u. Furthermore, we study a biaxial strain effect on the FM of the VI$_3$ monolayer. Our results show that the $a_{1g}\,{}^1e'_-^1$ ground state remains robust against the strains on the optimized lattice (see the blue curve in the inset of Fig. 4). The FM superexchange strength rises in the feasible tensile strain (e.g., up to 5%) but decreases in the compressive strain (see the red curve). Then, assuming a feasible biaxial tensile strain, and using the increasing FM superexchange strength and Ising magnetism associated with the robust $a_{1g}\,{}^1e'_-^1$ ground state, we carry out Monte Carlo simulations to estimate T_C in the 2D Ising FM VI$_3$ monolayer. As seen in Fig. 4, T_C increases from 70 K for the bare VI$_3$
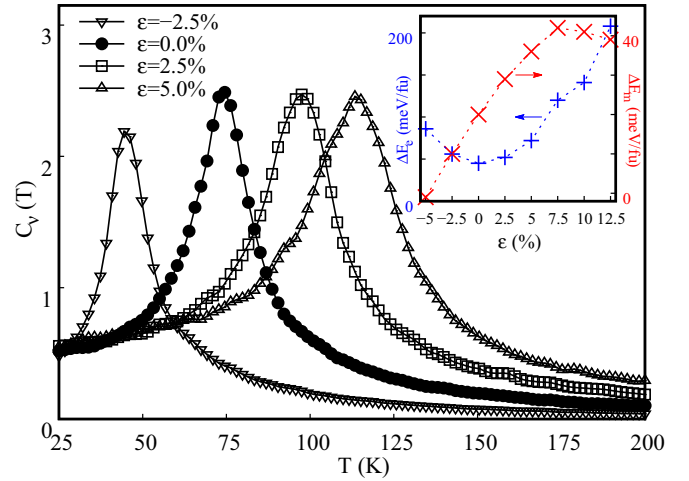

FIG. 4. Monte Carlo simulations of the specific heat of the VI$_3$ monolayer under strains. The inset shows the relative stability of the $a_{1g}\,{}^1e'_-^1$ ground state against the $e'^2_\pm$ state (blue curve), and the FM stability of the $a_{1g}\,{}^1e'_-^1$ ground state against the AF state (red curve).

monolayer to 90 K at 2.5% strain, and to 110 K at 5% strain (but decreases to 45 K at −2.5% strain). Therefore, the VI$_3$ monolayer could be the first Ising-type 2D FM with a pretty high T_C, particularly under a biaxial tensile strain. This prediction calls for a prompt experimental verification.

The present case, VI$_3$, in comparison with the extensively studied CrI$_3$ [1,4–13], demonstrates the importance of orbital degrees of freedom (orbital degeneracy) in promoting novel exotic properties of 2D magnets. Whereas in CrI$_3$ without orbital degeneracy the SIA is negligible and the FM ordering in single layers is due to the weak exchange anisotropy [12,13], in the presence of orbital freedom as in VI$_3$ we get the significant Ising character already at a single-ion level. Thus we can propose that using orbital degrees of freedom may strongly enrich magnetic properties of, in particular, 2D magnets. Considering the common honeycomb structure of layered materials, the moderate (stronger) trigonal crystal field of the local octahedral $3d$ ($4d$) transition metal ions with partially filled t_{2g} shells may favor a large orbital moment (in principle, $L_z = 1$ in size) and thus a strong perpendicular SIA, e.g., for high-spin $3d^2$ ($S = 1$, $a_{1g}\,{}^1e'^1$), $3d^6$ ($S = 2$, $e'^3 a_{1g}\,{}^1e^2$), and $3d^7$ ($S = 3/2$, $a_{1g}\,{}^2e'^3 e^2$), and for $4d^2$ ($S = 1$, $a_{1g}\,{}^1e'^1$) and low-spin $4d^4$ ($S = 1$, $e'^3 a_{1g}^1$). Here the $S = 1/2$ ionic states are not listed as their magnetic coupling may not be sufficiently strong due to the small spins. The $5d$ ionic states are not discussed here as they are often nonmagnetic or weakly spin polarized due to the strong crystal field and significant covalency with the ligands. Then one could make use of these $S \geqslant 1$ ionic states with strong SIA, as well as the above superexchange pictures associated with different orbitals, to search more 2D Ising magnets.

In summary, 2D FM materials are desirable for spintronics. Here we have demonstrated, through DFT calculations (LSDA+SOC+U), crystal field level analyses, and superexchange pictures, that the VI$_3$ monolayer has the $a_{1g}\,{}^1e'_-^1$ ground state with a significant SIA and enhanced FM couplings. This unique state produces an Ising-type FM. Our results well account for the experimental hard perpendicular

FM in bulk VI$_3$. Moreover, we predict, based on the MC simulations, that the VI$_3$ monolayer could well be the first 2D Ising FM with a pretty high T_C, particularly under a biaxial tensile strain. Furthermore, we suggest a group of spin-orbital states with a strong SIA which may help to search more 2D Ising magnets.

[1] B. Huang, G. Clark, E. Navarro-Moratalla, D. R. Klein, R. Cheng, K. L. Seyler, D. Zhong, E. Schmidgall, M. A. McGuire, D. H. Cobden, W. Yao, D. Xiao, P. Jarillo-Herrero, and X. Xu, Nature (London) **546**, 270 (2017).

[2] C. Gong, L. Li, Z. Li, H. Ji, A. Stern, Y. Xia, T. Cao, W. Bao, C. Wang, Y. Wang, Z. Q. Qiu, R. J. Cava, S. G. Louie, J. Xia, and X. Zhang, Nature (London) **546**, 265 (2017).

[3] Y. Deng, Y. Yu, Y. Song, J. Zhang, N. Z. Wang, Z. Sun, Y. Yi, Y. Z. Wu, S. Wu, J. Zhu, J. Wang, X. H. Chen, and Y. Zhang, Nature (London) **563**, 94 (2018).

[4] B. Huang, G. Clark, D. R. Klein, D. MacNeill, E. Navarro-Moratalla, K. L. Seyler, N. Wilson, M. A. McGuire, D. H. Cobden, D. Xiao, W. Yao, P. Jarillo-Herrero, and X. Xu, Nat. Nanotechnol. **13**, 544 (2018).

[5] S. Jiang, J. Shan, and K. F. Mak, Nat. Mater. **17**, 406 (2018).

[6] Z. Sun, Y. Yi, T. Song, G. Clark, B. Huang, Y. Shan, S. Wu, D. Huang, C. Gao, Z. Chen, M. McGuire, T. Cao, D. Xiao, W. Liu, W. Yao, X. Xu, and S. Wu, Nature (London) **572**, 497 (2019).

[7] C. Huang, J. Feng, F. Wu, D. Ahmed, B. Huang, H. Xiang, K. Deng, and E. Kan, J. Am. Chem. Soc. **140**, 11519 (2018).

[8] M. Gibertini, M. Koperski, A. F. Morpurgo, and K. S. Novoselov, Nat. Nanotechnol. **14**, 408 (2019).

[9] T. Song, X. Cai, M. W. Tu, X. Zhang, B. Huang, N. P. Wilson, K. L. Seyler, L. Zhu, T. Taniguchi, K. Watanabe, M. A. McGuire, D. H. Cobden, D. Xiao, W. Yao, and X. Xu, Science **360**, 1214 (2018).

[10] M. A. McGuire, H. Dixit, V. R. Cooper, and B. C. Sales, Chem. Mater. **27**, 612 (2015).

[11] H. Wang, F. Fan, S. Zhu, and H. Wu, Europhys. Lett. **114**, 47001 (2016).

[12] J. L. Lado and J. Fernández-Rossier, 2D Mater. **4**, 035002 (2017).

[13] D.-H. Kim, K. Kim, K.-T. Ko, J. H. Seo, J. S. Kim, T.-H. Jang, Y. Kim, J.-Y. Kim, S.-W. Cheong, and J.-H. Park, Phys. Rev. Lett. **122**, 207201 (2019).

[14] T. Kong, K. Stolze, E. I. Timmons, J. Tao, D. Ni, S. Guo, Z. Yang, R. Prozorov, and R. J. Cava, Adv. Mater. **31**, 1808074 (2019).

[15] S. Son, M. J. Coak, N. Lee, J. Kim, T. Y. Kim, H. Hamidov, H. Cho, C. Liu, D. M. Jarvis, P. A. C. Brown, J. H. Kim, C.-H. Park, D. I. Khomskii, S. S. Saxena, and J.-G. Park, Phys. Rev. B **99**, 041402(R) (2019).

[16] S. Tian, J. F. Zhang, C. Li, T. Ying, S. Li, X. Zhang, K. Liu, and H. Lei, J. Am. Chem. Soc. **141**, 5326 (2019).

[17] J. Yan, X. Luo, F. C. Chen, J. J. Gao, Z. Z. Jiang, G. C. Zhao, Y. Sun, H. Y. Lv, S. J. Tian, Q. W. Yin, H. C. Lei, W. J. Lu, P. Tong, W. H. Song, X. B. Zhu, and Y. P. Sun, Phys. Rev. B **100**, 094402 (2019).

[18] E. Gati, Y. Inagaki, T. Kong, R. J. Cava, Y. Furukawa, P. C. Canfield, and S. L. Bud'ko, Phys. Rev. B **100**, 094408 (2019).

[19] P. Doležal, M. Kratochvílová, V. Holý, P. Čermák, V. Sechovský, M. Dušek, M. Míšek, T. Chakraborty, Y. Noda, S. Son, and J.-G. Park, Phys. Rev. Mater. **3**, 121401(R) (2019).

[20] Y. Liu, M. Abeykoon, and C. Petrovic, Phys. Rev. Res. **2**, 013013 (2020).

[21] P. Blaha, K. Schwarz, G. Madsen, D. Kvasnicka, and J. Luitz, Wien2k package, http://www.wien2k.at.

[22] See Supplemental Material at http://link.aps.org/supplemental/10.1103/PhysRevB.101.100402 for (i) computational details, (ii) cleavage energy, and (iii) LDA, LSDA, and LSDA+U results.

[23] V. I. Anisimov, F. Aryasetiawan, and A. I. Lichtenstein, J. Phys.: Condens. Matter **9**, 767 (1997).

[24] N. Metropolis and S. Ulam, J. Am. Stat. Assoc. **44**, 335 (1949).

[25] J. He, S. Ma, P. Lyu, and P. Nachtigall, J. Mater. Chem. C **4**, 2518 (2016).

[26] X. Ou, H. Wang, F. Fan, Z. Li, and H. Wu, Phys. Rev. Lett. **115**, 257201 (2015).

[27] X. Ou and H. Wu, Sci. Rep. **4**, 4609 (2014).

[28] G.-Q. Liu, V. N. Antonov, O. Jepsen, and O. K. Andersen, Phys. Rev. Lett. **101**, 026408 (2008).

[29] M. W. Haverkort, I. S. Elfimov, L. H. Tjeng, G. A. Sawatzky, and A. Damascelli, Phys. Rev. Lett. **101**, 026406 (2008).

[30] S. Grimme, J. Comput. Chem. **27**, 1787 (2006).

[31] X. Li and J. Yang, J. Mater. Chem. C **2**, 7071 (2014).

[32] D. I. Khomskii, *Transition Metal Compounds* (Cambridge University Press, Cambridge, UK, 2014).